PROCEEDINGS, 45th Workshop on Geothermal Reservoir Engineering
Stanford University, Stanford, California, February 10-12, 2020
SGP-TR-216

Deformation, Failure and Permeability Evolution of Sealed Fractures in EGS Collab Poorman Schist

Zhi YE[1], Ahmad GHASSEMI[1], Tim KNEAFSEY[2]

1. Reservoir Geomechanics and Seismicity Research Group, The University of Oklahoma, Norman, OK 73069

2. Energy Geosciences Division, Lawrence Berkeley National Laboratory

ahmad.ghassemi@ou.edu

Keywords: EGS Collab, Stimulation, Sealed fractures, Foliations, Reactivation, Permeability

ABSTRACT

It is widely recognized that reactivation of pre-existing fractures by injection can play a crucial role in permeability creation during EGS stimulation. A numbers of previous studies have focused on the permeability enhancement by shear slip and propagation of open fractures in response to injection. The contributions of sealed fractures (e.g. filled fractures, foliations, and veins) to permeability creation during hydraulic injection have not scrutinized. These weak planes are supposedly reactivated by injection to provide high conductive flow paths and potentially form a network by coalescence with hydraulic fractures. In this work, a Poorman Schist sample containing a calcite-filled vein and foliations from the EGS Collab site (Sanford Underground Research Facility) was used to conduct laboratory injection tests. The test included four steps: (1) potential for jetting flows similar to those observed in Collab stimulation tests; (2) characterization of the sample permeability before reactivation/stimulation; (3) reactivation of a relatively thick vein (mineralized sealed fracture) in the sample by pressurized fluid; and (4) evaluation of permeability enhancement by the reactivation of the fracture. The results demonstrated that the sealed fracture or vein is more permeable than the rock matrix and the jetting flows observed in Collab stimulation site could be related to such natural discontinuities. In addition, the foliation planes are relatively weaker and can be reactivated by fluid injection before the vein/sealed fractures, resulting in flow rate/permeability enhancement. The failure behavior and the temporal-spatial evolution of AE hypocenters during the test indicate that natural discontinuities (foliation, and veins) increase the complexity of hydraulic stimulation (fracturing and shear stimulation) in Collab stimulation at Poorman Schist formation.

1. INTRODUCTION

The EGS Collab project conducts meso-scale hydraulic stimulation and interwell flow experiments at Sanford Underground Research Facility (SURF) to characterize rock failure behavior and probe the fluid-flow and heat transfer process for geothermal reservoir development (Kneafsey et al., 2018, 2019). EGS Collab Experiment 1 boreholes are entirely within the Poorman Formation, a metasedimentary rock consisting of sericite-carbonate-quartz phyllite (the dominant rock type), biotite-quartz-carbonate phyllite, and graphitic quartz-sericite phyllite (Caddey et al., 1991). Carbonate minerals present consist of calcite, dolomite, and ankerite. The rock is highly deformed and contains carbonate, quartz veins/boudinage, pyrrhotite, and minor pyrite. Other mineral phases (in addition to those listed above) include graphite and chlorite. The Poorman schists contains different type of discontinuities such as open and sealed natural fractures, foliations planes, and different mineralization bands distributed at different scales (Uzunlar, 2019). The mechanical deformation, failure behavior, and transport properties of subsurface rock mass are highly influenced by these natural discontinuities and fabric features. In our previous work (Ye, Ghassemi, & Kneafsey, 2019), we have carried out laboratory injection tests on Poorman Schist sample with an open fracture to characterize its seismo-hydro-mechanical response during fracture shear slip. The results demonstrated that the open fractures in Poorman Schist can be reactivated and propped by pressurized fluid injection for permeability enhancement. Creating permeability by the shear reactivation of pre-existing fractures has been known for a long time. However, most previous experiments have focused on the permeability enhancement by shear slip and propagation of open fractures in response to injection (Esaki et al., 1999; Ishibashi et al., 2016; Park et al., 2013; Vogler et al., 2016; Ye & Ghassemi, 2018, 2019). The contributions of sealed fractures (e.g. filled fractures, foliations, and veins) to permeability creation during hydraulic stimulation have not been examined. Specifically, in Collab stimulation experiments it is observed that the hydraulic fractures tend to have complexity, involving multiple failure planes. In this paper, from the perspective of reservoir geomechanics, we used the term of *sealed fractures* to represent the natural discontinuities that are closed or partially/completely sealed by minerals. In general, the sealed fractures are likely more conductive and weaker than the rock matrix, and can supposedly be reactivated by injection to provide high conductive flow paths and potentially form a network by coalescence with hydraulic fractures.

In this work, we conducted laboratory triaxial injection test on a cylindrical Poorman Schist sample (containing a mineral-filled vein and multiple foliation planes) from EGS Collab site to characterize the deformation, failure and permeability evolution of the sample in response to fluid injection. First, we explored the potential for the jetting flows (observed by downhole camera in Collab stimulation tests) in the laboratory. The permeability of the vein and the equivalent permeability of the sample were then characterized using a fluid flow test under hydrostatic compression. Next, the sample was subjected to injection via a borehole to reactivate the vein (or other discontinuities) with concurrent acoustic emission (AE) monitoring, characterizing its seismo-hydro-mechanical response. The post-stimulated permeability of the sample was subsequently evaluated to explore the possible contribution of sealed fracture reactivation on permeability creation in Collab stimulation.

2. SAMPLE MATERIALS AND PREPARATION

The sample used in this experimental study is a cylindrical Poorman Schist specimen having a 61 mm (2.4-inch) diameter and 110 mm (4.3-inch) length. The sample is from the 99.3 ft. – 100.25 ft. interval of well E1-PDT at EGS Collab Test Bed 1. As shown in Figure 1(a) and Figure 1(c), the sample (hereinafter sample PS-1) has a cross-cutting thick vein (~10 mm thick) and multiple foliation planes of various thicknesses (from ~1 to ~3 mm). Based on reaction with hydrochloric acid, the vein contains abundant calcite mineral. The mineralogical composition of the Poorman Schist was determined by X-ray diffraction analysis at School of Geoscience, University of Oklahoma. Results show the Poorman Schist sample consists of calcite (30.6%), quartz (22.7%), clinochlore (20.2%), and dolomite (17.7%), with a few percentages of annite (6.1%) and muscovite (2.7%). The vein makes an angle of 30º with respect to horizontal axis of the sample, while the foliation layers have a slightly larger inclination (the inclination angle is ~35º from the foliations to the horizontal axis of the sample, see CT image in Figure 1(c)). To measure the transport properties of the vein, two 3.5 mm diameter vertical boreholes (see Figure 1(b)), 6 mm from the sidewall, were drilled (using a diamond drill bit) from each end surface of the cylindrical sample to reach the vein and to form a flow path. The two boreholes did cross the thick vein.

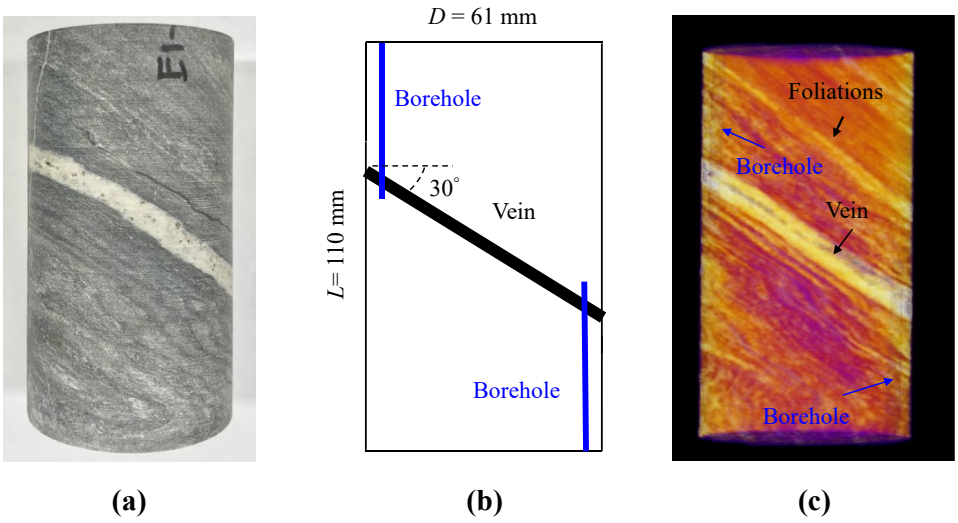

Figure 1: (a) Poorman Schist sample from E1-PDT 99.3 ft. – 100.25 ft.; (b) the geometry of calcite-filled vein and predrilled boreholes; (c) CT scanning image of the sample (the sample was CT scanned at Berkeley Lab).

3. JET FLOWS IN LABORATORY INJECTION TEST

Three hydraulic characterization tests were conducted in EGS Collab Experiment 1 to quantify hydraulic characteristics of the stimulated fracture system connecting E1-I and E1-P. One of the primary objectives of the hydraulic characterization tests is to locate fluid entry points in E1-P from the hydraulic stimulation in E1-I. A downhole camera was deployed for identifying the fluid entry points in E1-P, and the downhole camera logging in E1-P detected a couple of jetting flow points at the wellbore interval from 126 ft. to 130 ft. (Kneafsey et al., 2019). One can speculate the jetting flows into the production wellbore are from the partially-open natural discontinuities. As shown in Figure 2, several fluid entry points can be observed in the wellbore as jetting points. Moreover, it is observed that these jetting flow points are located on a white-color band, which is quite similar (but appear thinner) to the white vein in Figure 1(a). An interpretation is that the pre-existing discontinuity band is partially opened to provide a preferable flow path for the water injected from the well E1-I.

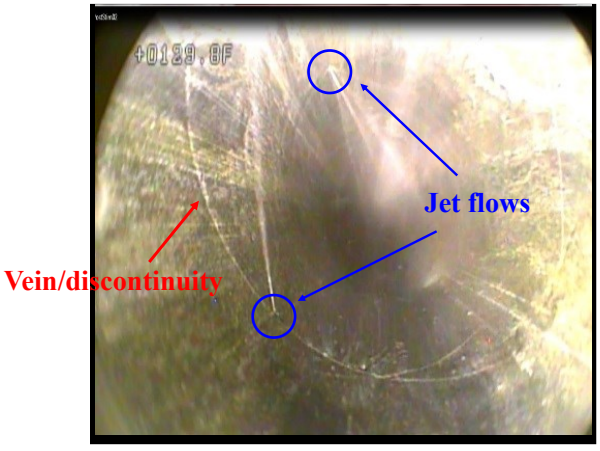

Figure 2: Downhole camera image showing the fluid jetting points (blue circles) in wellbore of E1-P at 129.15 ft.

To test the potential mechanism of jet flows observed in the production wellbore, a laboratory analog test was conducted in the Poorman Schist sample PS-1 (from the production well E1-PDT) under ambient pressure and temperature. As illustrated in Figure 3(a), the two sample ends were sealed by epoxy. In the test, the prepared sample was axially loaded by the MTS 810 test System with a ~10 MPa axial stress. Water was injected into the vein from the bottom end of the sample through the pre-drilled borehole at a flow rate of 10 ml/min. The top sample end connecting with the vein by another borehole was sealed so that fluid only can flow out through the sidewall of the sample. A high-speed camera was used to monitor and identity the fluid outlet points.

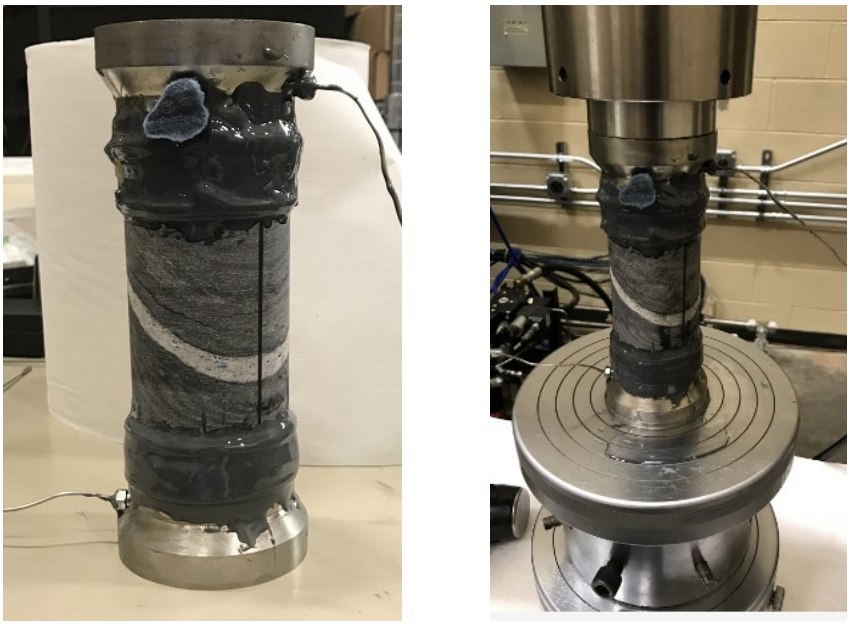

(a) **(b)**

Figure 3: Fluid flow test under ambient pressure and room temperature for revealing the possible mechanism of jet flows in EGS Collab Experiment 1: (a) sample configuration; (b) the experimental setup in MTS 810 Test System.

As can be seen in Figure 4, at least two jet flows emanate from the vein in sample PS-1. This means that the vein has a relatively higher conductivity than the rock matrix, and some open pores or "karst" in the vein create a preferable flow path for the fluid. The jet flows replicated in the laboratory test are quite similar as that observed in the EGS Collab Experiment 1. Considering the broad existence of natural discontinuities in Poorman Schist, sealed fractures could highly influence the stimulation process and fluid flow in EGS Collab Experiments.

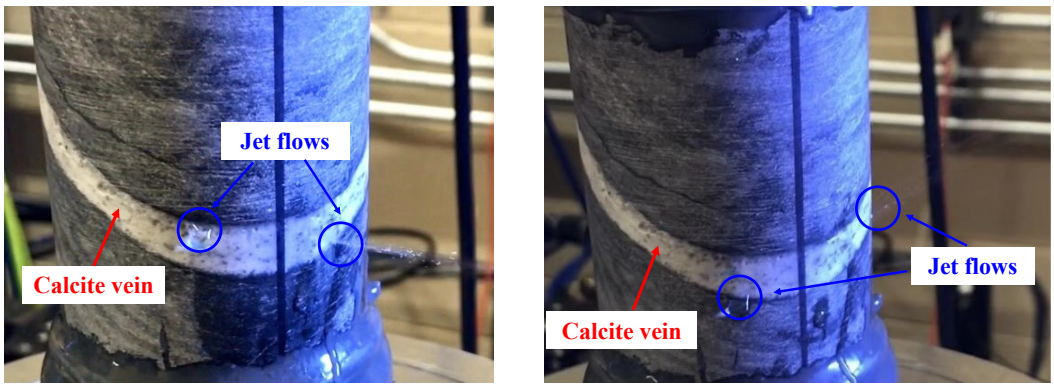

(a) **(b)**

Figure 4: Jet flows replicated in laboratory injection test: (a) image of jet flows at t = 56 s; (a) image of jet flows at t = 72 s.

4. CHARACTERIZATION OF PRE-STIMULATED PERMEABILITY

Results of the above fluid flow test under ambient pressure demonstrated the vein to be permeable with larger permeability than that of the rock matrix. Therefore, it is of interest to better characterize the pre-stimulated permeability of the vein and the sample. We carried out a triaxial-injection test on sample PS-1 to measure the in-situ permeability of the vein and the sample. The sample was jacketed by a copper sheet with 1.27 mm thickness, and then subjected to a hydrostatic compression with a 21.7 MPa confining pressure (in-situ

minimum horizontal principal stress). As illustrated in Figure 5, two Teledyne ISCO 100DM syringe pumps separately connected with the top and bottom ends of the sample were used to inject and produce fluid. The initial injection pressure in pump A and the production pressure in pump B were set as 4 MPa. During the test, the production pressure was kept constant, while the injection pressure was increased stepwise to create a pressure potential between the injection and production boreholes. As a result, water circulated from pump A to pump B. The stepwise elevation of the injection pressure was employed to investigate the evolution of steady-state permeability. Each injection pressure step lasted ~600 seconds including a pressure buildup stage which required ~200 seconds and a constant pressure hold stage which lasted another ~400 seconds. After the target injection pressure was achieved, the pressure was held constant for at least 200 seconds before recording the flow rate to ensure the flow rate measurement was in the steady-state flow regime. When the flow rate out of pump A was nearly identical to the flow rate into pump B (the difference of flow rates is less than 5%), we considered the fluid flow through the fracture to have reached a steady-state.

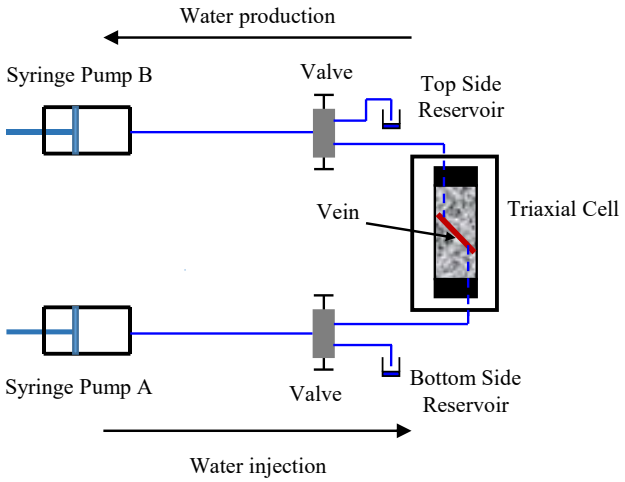

Figure 5: Fluid flow design for permeability characterization.

In the constant pressure (hold) stage of each step, when the injection flow rate is nearly equal to the production flow rate, and the steady-state flow regime is satisfied. Using Darcy's law, the equivalent permeability of the sample can be calculated as:

$$k_e = -\frac{\mu Q}{A}\cdot\frac{L}{\Delta P} = -\frac{4\mu Q}{\pi D^2}\cdot\frac{L}{\Delta P} \quad (1)$$

where, Q is the flow rate in steady-state regime, estimated by averaging the injection flow rate and production flow rate; ΔP (differential pressure) is the difference between injection pressure (P_i) and production pressure (P_o); μ is the fluid viscosity (1.002×10^{-3} Pa·s at 20 ºC for water); A is the cross-section area of the cylindrical shale sample ($A = \frac{1}{4}\pi D^2$); D and L are the sample diameter and sample length, respectively.

In the present injection test, the vein is elliptical or near elliptical (indicated by the black ellipse in Figure 6). To simplify the estimation of the vein permeability, the vein can be assumed as a fracture, and the elliptical fluid flow region is assumed as a *rectangle* (represented by the blue rectangle in Figure 6). The rectangle has a same area as the elliptical fracture surface. The length (L) of the rectangle is the distance between the two boreholes on fracture surface, and the width (W) of the rectangle is equal to the area (A) of the ellipse divided by the length (L) of the rectangle (see Ye & Ghassemi, 2018 for additional details in the approximation of fracture permeability).

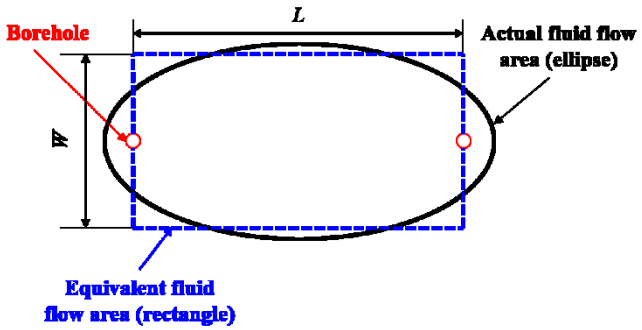

Figure 6: Fluid flow region for vein permeability estimation: the ellipse is the actual fluid flow region, while the rectangular area delineated by blue dotted lines is the equivalent fluid flow region.

According to the cubic law (Witherspoon et al., 1980; Zimmerman & Bodvarsson, 1996), the vein used in the injection test is assumed as a parallel-sided fracture with an equivalent hydraulic aperture (a_h). The vein permeability (k_v) is further evaluated by:

$$k_f = \frac{a_h^2}{12} \tag{2}$$

where, k_v is the vein permeability evaluated by the cubic law; a_h is the equivalent hydraulic aperture of the vein.

Considering the flow into the low permeability matrix is very small, and the gravity effect is negligible, the steady-state flow rate (Q) is represented using Darcy's law:

$$Q = -\frac{W a_h^3}{12\mu} \cdot \frac{\Delta P}{L} \tag{3}$$

where, Q is the steady-state flow rate under the constant injection pressure hold stage; ΔP is the differential pressure; μ is the fluid viscosity (1.002×10^{-3} Pa·s at 20 ºC for water); W and L are the vein width and length estimated from the rectangular fluid flow regime in Figure 6, respectively.

Therefore, the equivalent hydraulic aperture (a_h) of the fracture is estimated using the measurements in steady-state flow regime:

$$a_h = \left(-\frac{12\mu LQ}{W\Delta P}\right)^{1/3} \tag{4}$$

In the fluid flow test under hydrostatic condition (with 21.7 MPa confining pressure), due to the low permeability before stimulation, the fluid flow could not reach steady-state unless the injection pressure was higher than 14 MPa. Therefore, the steady-state flow rates were measured in four steps with injection pressures of 14, 16, 18 and 28 MPa, respectively. The measurements of flow rate and permeability estimations under each injection pressure step are listed in Table 1. The permeability of the vein (k_v) is in the range of 5×10^{-15} m^2 to 8×10^{-15} m^2 (or 5 to 8 mDarcy), while the equivalent sample permeability (k_e) in the range of 5×10^{-20} m^2 to 1×10^{-19} m^2 (or 50 to 100 nDarcy). Also it is observed that both the vein permeability and the equivalent sample permeability tend to linearly increase with the elevation of injection pressure (see Figure 7).

Table 1: The estimations of vein permeability and equivalent sample permeability.

P_i (MPa)	P_o (MPa)	Q (ml/min)	k_v ($\times10^{-15}$ m^2)	k_e ($\times10^{-19}$ m^2)
14	4	0.0008	5.11	0.50
16	4	0.0012	5.93	0.63
18	4	0.0015	6.21	0.67
20	4	0.0027	8.41	1.06

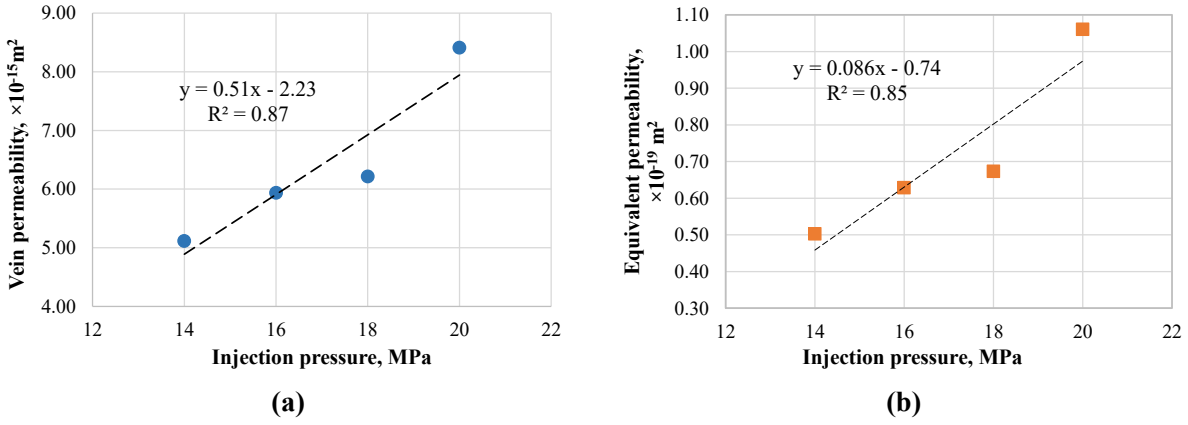

Figure 7: Linear relationships between injection pressure and (a) vein permeability and (b) equivalent sample permeability.

5. REACTIVATION OF SEALED FRACTURES BY PRESSURIZED FLUID INJECTION

The next step is to reactivate the sealed fracture by pressurized fluid injection and evaluate the permeability evolution after the reactivation, which aims to reveal the role of sealed fractures in Collab stimulation and permeability creation. Before the test it was anticipated that the thick vein would fail and become reactivated. As shown in Figure 8(a), two Linear Variable Differential Transformer (LVDT) position sensors and the third LVDT mounted on a ring were used to measure the average axial deformation and the radial deformation of the sample, respectively. Eight piezoelectric transducers of diameter 7 mm and 500 kHz resonant frequency were bonded to the copper jacket with conductive epoxy in the arrangement shown in Figure 8(b). The AE (acoustic emission) instrument used in this study is an Express-8 AE system supplied by PAC. The AE test setup consists of crystal transducers, 2/4/6 preamplifiers, processing instrumentation, and AE win software. During the test, the electrical signals from each of the crystal transducers were amplified by the 2/4/6 preamplifiers and passed through an analog filter operating between 5 kHz and 400 kHz. After

the filter, each of the signals (voltages) then was measured if above a threshold level of 45 dB with a 10 MSPS sampling rate (high sampling rate).

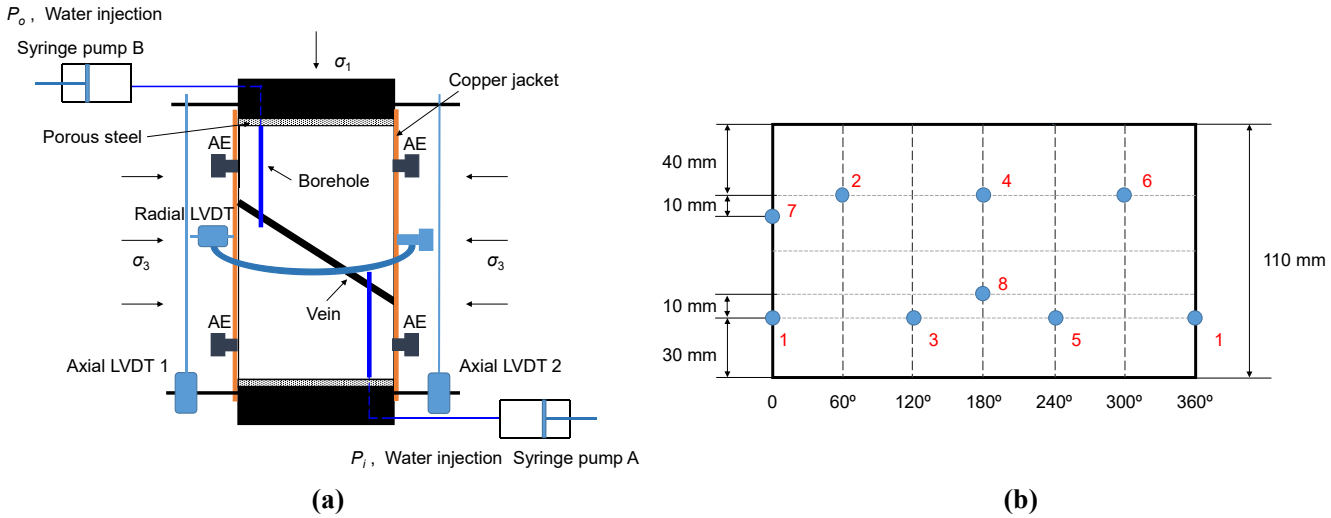

Figure 8: Reactivation of sealed fracture by injection: (a) experimental setup; (b) projected sample surface showing the location of 8 piezoelectric crystal transducers for AE monitoring (the blue circles indicate the transducers). The black line in the left plot represents the fracture. AE=Acoustic Emission, LVDT= Linear Variable Differential Transformer.

In the test, after applying a 21.7 MPa (σ_3) confining pressure to the sample, the production pressure of pump B (P_o) was fixed to a constant value of 4 MPa, and the injection pressure of pump A (P_i) was set to an initial value of 4 MPa and later was increased to reactivate the sealed fractures (or weak planes). The sample was then loaded (using a displacement rate of 0.01 mm/s) to a near-critical condition with differential stress ($\sigma_d = \sigma_1 - \sigma_3$) of ~82 MPa (see Figure 9(a)), which can be determined from the dilation/deflection of the stress-volumetric strain curve (Figure 9(a), Ye & Ghassemi, 2016). This near-critical stress level should be large enough to cause the reactivation or failure of the sample during injection, but not exceed the strength to reactivate before injection starts. After that, the test was switched to the constant piston-displacement control mode used by Ye & Ghassemi (2017). The stressed sample was permitted to relax for at least 20 minutes, ensuring that no new AE events were induced and the fluid flow was stabilized in the fracture (with almost zero flow rate reading on the pump) before elevating injection pressure. Next, the injection pressure was gradually increased at a rate of 0.5 MPa/s to induce the reactivation of the vein or foliations. The injection pressure was kept constant when the reactivation/failure was observed as indicated by the rapid increase of sample deformation. The mechanical parameters (displacement and stress), fluid flow parameters (pressure and flow rate), and AE activities (AE hits and events) were all concurrently measured to characterize the seismo-hydro-mechanical responses of the sample exposed to pressurized fluid injection.

The stress-strain curves during the loading stage are shown in Figure 9(a) and Figure 9(b). Using the mechanical measurements in loading stage, the Young's modulus and Poisson's ratio of the sample are determined to be 51.86 GPa and 0.32, respectively.

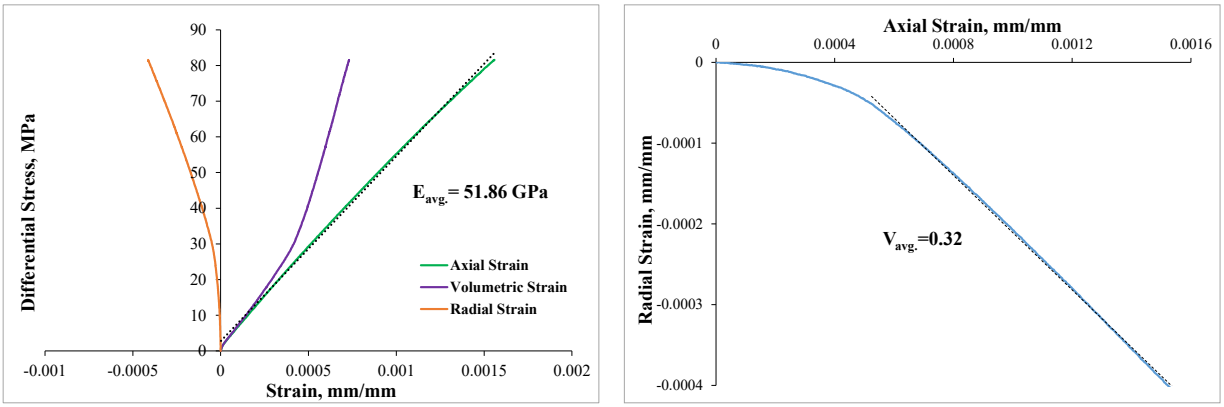

Figure 9: The stress –strain curves in the loading stage, indicating a 51.86 GPa Young's modulus and 0.32 Poisson's ratio (tangent values at a differential stress of 82 MPa).

The seismo-hydro-mechanical measurements during the injection test are shown in Figure 10. In the plots, the rock deformation and fluid flow in the pre-injection stages (initial applications of confining pressure, axial loading, and injection pressure) are not shown. This means that the displacements and flow rates were zeroed before elevating the injection pressure. Also, the corresponding acoustic emission activity in the pre-injection stage was not accounted. During the test, a total of 12 parameters were concurrently measured in response to fluid injection. As shown in Figure 10, the green curve represents the loading piston displacement of the MTS 816 frame, which remained constant under a constant piston-displacement control. The black curve describes the differential stress history which shows a significant drop once the sample having sealed fractures is reactivated. The blue curve is the injection pressure which was increased gradually from 4 MPa to 10 MPa at a rate of 0.5 MPa/s. The constant production pressure (P_o = 4 MPa) is represented by the gray curve. The red and pink curves are the axial shortening and radial expansion of the sample, respectively. The fluid volumes in the injection and production pumps are separately represented by the brown curve and the teal curve. The purple curve is the injection flow rate recorded by syringe pump A, and the dark-red curve is the production flow rate from syringe pump B. The cumulated AE hits and events are illustrated by the light-blue curve and the gold curve, respectively. It is noticed from the plots that the stresses, displacements, flow rates, and AE signals vary with the changes of injection pressure.

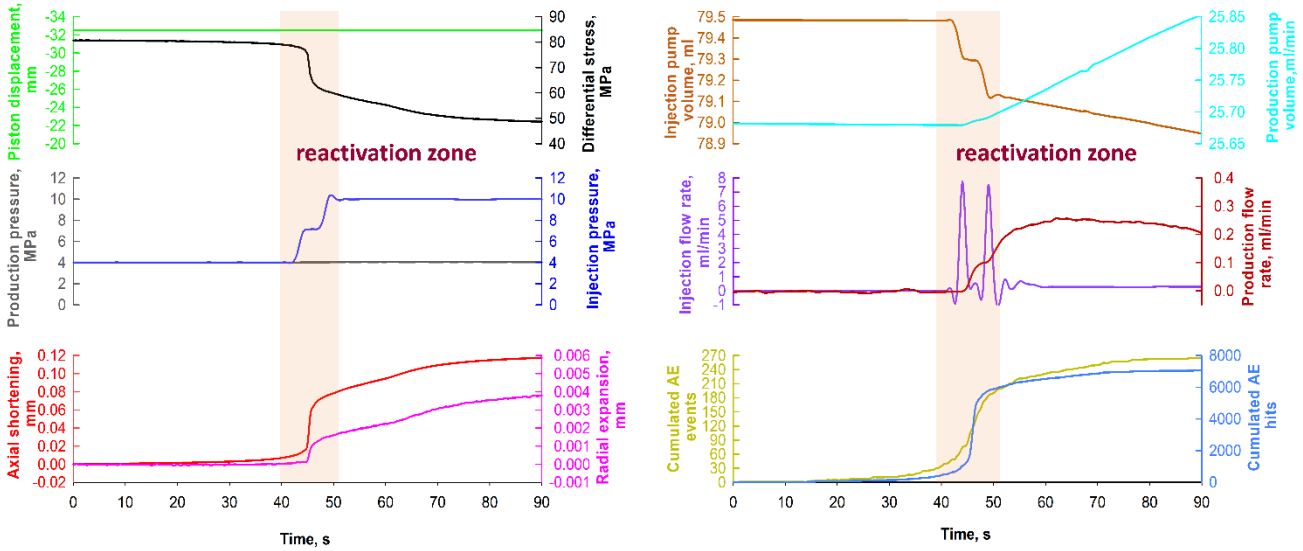

Figure 10: The seismo-hydro-mechanical measurements of sample PS-1 in response to pressurized fluid injection. The flattening of the injection pressure and production curves (during ~43 s to ~46 s) indicates failure of the foliation plane and creation of new volume in the sample.

As shown in Figure 10, the temporal evolution of the injection test can be roughly subdivided into three stages, corresponding with the changes of injection pressure and sample deformation. The major aspects of each stage with different hydro-mechanical response are discussed below:

- Stage 1: The injection pressure was kept as 4 MPa for ~40 s. In this stage, the sample has almost negligible axial and radial deformation. The energy stored within the sample is slightly released in a creeping manner accompanied with a limited numbers of AE hits and events. The flow rate in the two pumps are almost zero.
- Stage 2: In this pressurization stage (from ~40 s to ~52 s), the injection pressure was increased from 4 MPa to 10 MPa at a rate of 0.5 MPa/s. Then, the sample failed (likely by reactivation of the vein and/or foliations) as indicated by the sudden increase in the rates of both axial and radial deformations. As a result, a rapid stress drop (>20 MPa) occurred along with a large number of AE hits (>6000 hits) and AE events (>200 events). The flow rate and fluid volume in pump B gradually increased with the elevation of injection pressure. This means that water flowed from pump A to pump B due to the pressure difference between injection pump A and production pump B. In this stage, the injection fluid volume from pump A (~0.4 ml) is much larger than the production fluid volume in pump B (0.05 ml). Considering the low permeability of the sample before stimulation, this indicates that most of the injected fluid was stored into the *stimulated reservoir volume*.
- Stage 3: After the reactivation and sample failure, the injection pressure was kept as at constant 10 MPa for another ~40 s. The sample deformed with a moderate rate, corresponding to the gradually decreasing differential stress. More AE events were detected but with at a lower rate compared with that of the second stage. The fluid flow reached steady-state as indicated by the almost equal injection flow rate (0.27 ml/min) and the production flow rate (0.25 ml/min). This means that most of injected volume from pump A was produced from pump B, except small fraction stored in the stimulated sample.

Figure 11 shows the location of AE hypocenters and the failed sample (after the test). It is obseved that the tested sample PS-1 has failed along a visible plane dipping at ~35° with respect to the horizontal axis of the sample (see Figure 11 (b)) rather than along the thick vein. Comparison with the CT scan image of Figure 1(c) shows that the failure occurred along a foliation band. In the test, a total of 361 AE events were detected. Most of the induced AE events are located in the upper-right region, which matches well the toe of the failed foliation plane. This means that a large portion of AE events were induced during the reactivation along the foliation plane by injection.

In addition, some AE events were detected in a zone near the calcite vein. This indicates that mechanical deformation and micro-failures were also induced in the calcite vein by injection, although a visible macroscopic failure of the vein is not observed.

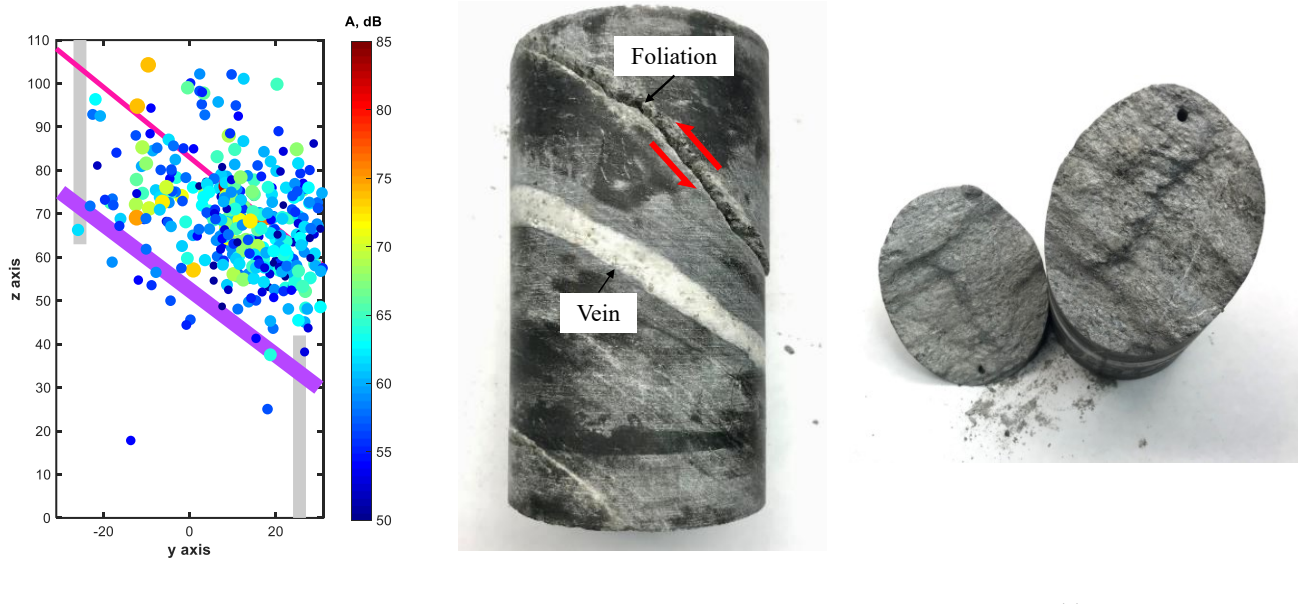

Figure 11: (a) The location of AE hypocenters in *x*-*z* plane; (b) the failed sample after test showing a reactivated foliation plane; (c) slickensides and produced gouges on the failed foliation plane. In the plot of AE location, the dots with different sizes indicate the AE events with different amplitudes (from 50 dB to 85 dB).

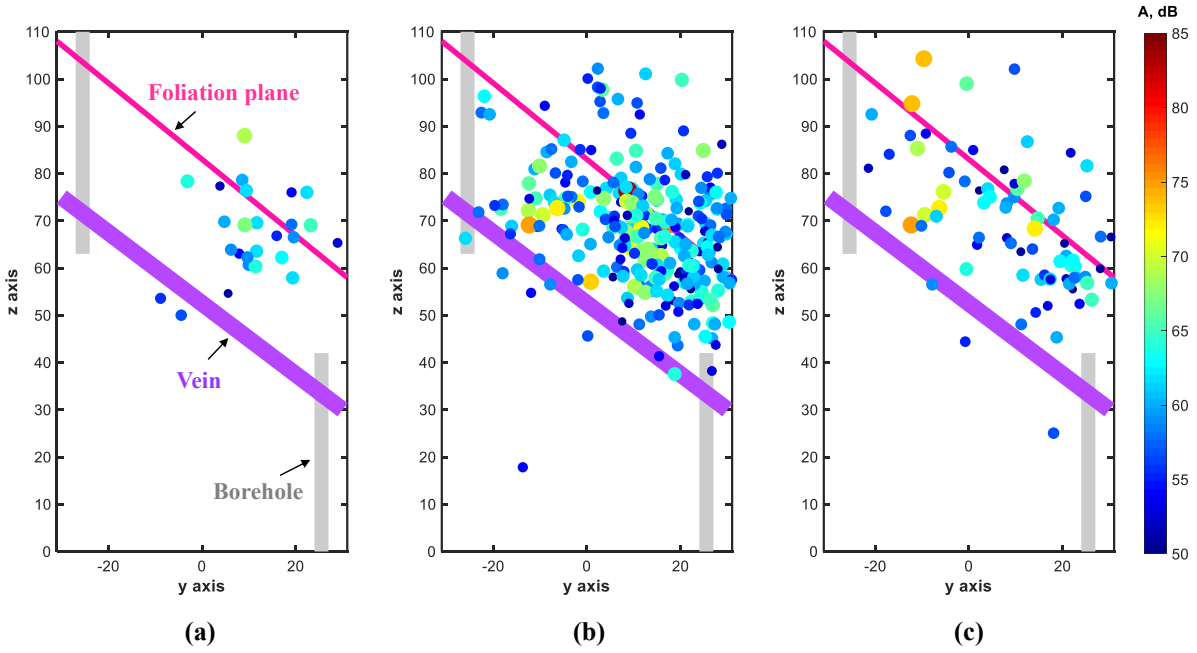

Figure 12: The temporal-spatial evolution of AE hypocenters in *x*-*z* plane: (a) 28 AE events were detected in stage 1 from 0 s to 40 s; (b) 285 AE events were detected in stage 2 from 40 s to 52 s; (c) 48 events were detected in stage 3 from 52 s to 90 s. In the plot of AE location, the dots with different sizes indicate the AE events with different amplitudes (from 50 dB to 85 dB).

The temporal evolution of AE hypocenters is shown in the Figure 12. It is found that 28 AE events were detected in stage 1 (from 0 s to 40 s), 285 AE events were monitored in stage 2 (from 40 s to 52 s), and 48 events were noticed in stage 3 (from 52 s to 90 s). This means that most of AE events are induced in the stage 2 of fluid pressurization, corresponding well with the large stress drop in the stage. The AE events in stage 1 have relatively low magnitudes (Figure 12(a)), since there was no major failure in this stage. The main shock occurred at 43 s in stage 2 (Figure 12(b)), with the largest AE magnitude of 83 dB, which correlates well with the largest sample deformation and rapid stress drop of stage 2. In stage 3, some large AE events with magnitudes over 70 dB were detected. A possible

explanation is that the failed foliation plane experienced further shear slip in stage 3, which is evidenced by the further sample deformation and stress drop in the test (Figure 10), and as well as by the gouge production and slickensides observed on the failed foliation plane (Figure 11 (c)). Considering the failure behavior and the evolution of AE hypocenters, it is concluded that the vein was stronger and less favorably oriented than the foliation plane. Furthermore, it appears that a portion of the fluid penetrated the matrix near the lower end of the vein and the pressure front entered the foliation plane above it, facilitating failure initiation at its toe and higher dipping zone. This interpretation is consistent with previous experiment studies that the foliations in Poorman Schist can serve as flow paths for fluid transport during Collab stimulations (Frash et al., 2019; Ye, Ghassemi, & Kneafsey, 2019). In the test, the injection pressure was increased at a constant rate of 0.5 MPa/s in stage 2 (from 40 s to 52 s), so the record of injection pressure (blue curve in Figure 10) should show a continually increasing trend. However, it is noticed that the injection pressure did not build-up during ~43 s to ~46 s time interval. Considering that water was first injected into the vein, and the foliation plane failed, a possible interpretation is that the foliation slipped during ~43 s to ~46 s. As a result, the sudden opening of the foliation plane took the injected fluid, and the injection pressure did not increase until it (or its available volume) was saturated. This observation is also consistent with the AE monitoring where the main shock occurred at ~43 s with largest AE magnitude of 83 dB, indicating the occurrence of a major failure.

6. CHRACTERIZATION OF POST-STIMULATED PERMEABILITY

To characterize the post-stimulated permeability of the sample, another flow test under hydrostatic compression (with 21.7 MPa confining pressure) was conducted on the failed sample. The results are listed in Table 2. Since both the foliation plane and the vein were taking fluid, we only report the equivalent permeability of the sample. The post-stimulation permeability of the sample is in the range of 3.25×10^{-17} m^2 to 3.56×10^{-17} m^2 (~30 μDarcy), indicating up to 3 orders of magnitude enhancement of permeability. This means that the reactivation of sealed fractures in Poorman Schist could significantly enhance the stimulated volume and the permeability.

Table 2: The estimations of equivalent sample permeability after the stimulation.

P_i (MPa)	P_o (MPa)	Q (ml/min)	k_e ($\times10^{-17}$ m^2)
12	4	0.31	3.25
14	4	0.42	3.30
16	4	0.56	3.52
18	4	0.68	3.56

7. CONCLUSIONS

In this study, we performed laboratory experiments on a Poorman Schist sample (containing sealed natural discontinuities) from the EGS Collab Experiment site to characterize its deformation, failure, and permeability evolution in response to injection. In the test, we first successfully replicated the jetting flows similar to those observed by downhole camera in field tests. The observations demonstrate that the natural discontinuities can be more permeable than the rock matrix, providing preferable fluid flow paths during fluid injection. Through a fluid flow test under hydrostatic compression, the permeability of the vein and the equivalent permeability of the sample before stimulation are estimated as ~10^{-15} m^2 (mDarcy) and ~10^{-20} m^2 (50 to 100 nDarcy), respectively. In addition, we carried out a stimulation test under triaxial loading on the sample with concurrent acoustic emission (AE) monitoring to characterize the seismo-hydro-mechanical response of the sample exposed pressurized fluid injection. The results indicated that the stressed Poorman Schist sample can be reactivated/failed at injection pressure below the minimum principal stress, matching with the concept of shear stimulation in EGS development. It is found the both the calcite vein and a foliation plane were reactivated by injection. The major failure occurred along the foliation plane. The failure behavior and the temporal-spatial evolution of AE events demonstrate that weaker foliation type discontinuities highly influence the mechanical and transport properties of Poorman Schist, and possibly increase the complex of hydraulic stimulation (fracturing and shear stimulation) in EGS Collab stimulation. The equivalent permeability of the sample after the *stimulation* increased to ~$\times10^{-17}$ m^2, which is ~3 orders of magnitude increase comparing with pre-stimulated permeability.

ACKNOWLEDGMENTS

This material was based upon work supported by the U.S. Department of Energy, Office of Energy Efficiency and Renewable Energy (EERE), Office of Technology Development, Geothermal Technologies Office, under Award Number DE-AC52-07NA27344 with LLNL, Award Number DE-AC05-76RL01830 with PNNL, and Award Number DE-AC02-05CH11231 with LBNL. The United States Government retains, and the publisher, by accepting the article for publication, acknowledges that the United States Government retains a non-exclusive, paid-up, irrevocable, world-wide license to publish or reproduce the published form of this manuscript, or allow others to do so, for United States Government purposes. The research supporting this work took place in whole or in part at the Sanford Underground Research Facility in Lead, South Dakota. The assistance of the Sanford Underground Research Facility and its personnel in providing physical access and general logistical and technical support is acknowledged. We also appreciate the efforts of the EGS Collab Team members.

REFERENCES

Caddey, S.W., et al.: The Homestake Gold Mine, An Early Proterozoic Iron-Formation-Hosted Gold Deposit, Lawrence County, South Dakota, U.S. Geological Survey, (1991), 67p.

Esaki, T., et al.: Development of a Shear-Flow Test Apparatus and Determination of Coupled Properties for A Single Rock Joint, *International Journal of Rock Mechanics and Mining Sciences*, **36**(5), (1999), 641-650.

Frash, L., et al.: EGS Collab Experiment 1 Geomechanical and Hydrological Properties by Triaxial Direct Shear, *Proceedings*, 44th Workshop On Geothermal Reservoir Engineering, Stanford, CA (2019).

Ishibashi, T., et al.: Exploring the Link between Permeability and Strength Evolution during Fracture Shearing, *Proceedings*, 50th U.S. Rock Mechanics/Geomechanics Symposium, Houston, TX (2016).

Kneafsey, T., et al.: An Overview of the EGS Collab Project: Field Validation of Coupled Process Modeling of Fracturing and Fluid Flow at the Sanford Underground Research Facility, Lead, SD, *Proceedings*, 43rd Workshop On Geothermal Reservoir Engineering, Stanford, CA (2018).

Kneafsey, T., et al.: EGS Collab Project: Status and Progress, *Proceedings*, 44th Workshop On Geothermal Reservoir Engineering, Stanford, CA (2019).

Park, H., et al.: Development of Coupled Shear-Flow-Visualization Apparatus and Data Analysis, *International Journal of Rock Mechanics and Mining Sciences,* ***63***, (2013), 72-81.

Uzunlar, N. 2019. Personal Communication with A. Ghassemi (2019).

Vogler, D., et al.: Permeability Evolution in Natural Fractures Subject to Cyclic Loading and Gouge Formation, *Rock Mechanics and Rock Engineering,* ***49***(9), (2016), 3463-3479.

Ye, Z., & Ghassemi, A.: Deformation Properties of Saw-Cut Fractures in Barnett, Mancos and Pierre Shales, *Proceedings*, 50th US Rock Mechanics / Geomechanics Symposium, Houston, TX (2016).

Ye, Z., & Ghassemi, A.: Injection-Induced Propagation and Coalescence of Pre-Existing Fractures in Granite Under Triaxial Stress, *Journal of Geophysical Research: Solid Earth*, **124** (8), (2019), 7806-7821.

Ye, Z., & Ghassemi, A.: Injection-Induced Shear Slip and Permeability Enhancement in Granite Fractures, *Journal of Geophysical Research: Solid Earth*, **123** (10), (2018), 9009-9032.

Ye, Z., Ghassemi, A., and Kneafsey, T.: Failure Behavior of the Poorman Schist and Its Fractures from EGS Collab Stimulation Site, *Proceedings*, 44th Workshop On Geothermal Reservoir Engineering, Stanford, CA (2019).

Ye, Z., Janis, M., and Ghassemi, A.: Injection-driven Shear Slip and The Coupled Permeability Evolution of Granite Fractures for EGS Stimulation, *Proceedings*, 51st US Rock Mechanics / Geomechanics Symposium, San Francisco, CA (2017).